

ACCOUNTING FOR ECCENTRICITY IN COMPRESSOR PERFORMANCE PREDICTIONS

Anna M. Young*, Teng Cao,

Ivor J. Day and John P. Longley

Whittle Laboratory

University of Cambridge, UK

Email: amy21@cam.ac.uk, tc367@cam.ac.uk,

ijd1000@cam.ac.uk, jpl1000@cam.ac.uk

ABSTRACT

In this paper, experiments and numerical modelling are used to quantify the effects of clearance and eccentricity on compressor performance and to examine the influence of each on flow distribution and stall margin.

A change in the size of the tip-clearance gap influences the pressure rise and the stall margin of a compressor. Eccentricity of the tip-clearance gap then further exacerbates the negative effects of increasing tip-clearance. There are few studies in the literature dealing with the combined effect of clearance and eccentricity. There is also little guidance for engine designers, who have traditionally used rules of thumb to quantify these effects. One such rule states that the stall margin of an eccentric machine will be equal to that of a concentric machine with uniform clearance equal to the maximum eccentric clearance. In this paper, this rule of thumb is checked using experimental data and found to be overly pessimistic.

In addition, eccentric clearance causes a variation in axial velocity around the circumference of the compressor. The current study uses a three dimensional model which demonstrates the importance of radial flow gradients in capturing this redistribution. Flow redistribution has been treated analytically in the past, and for this reason the modelling has been restricted to two dimensions.

The circumferential variation in axial velocity is also examined in terms of the local stability of the flow by considering the stalling flow coefficient of an equivalent axisymmetric compressor with the same local tip-clearance. The large clearance sector of the annulus is found to operate beyond its equivalent axisymmetric stall limit, which means that the small clearance sector of the annulus must be stabilising the large clearance sector. An improved rule of thumb dealing with the effects of eccentricity is presented.

INTRODUCTION

There are several sources of tip-clearance eccentricity in an aero-engine. These can be divided into two categories: transient and permanent [1]. Transient changes in clearance distribution are caused by gyroscopic effects during manoeuvres and by lifting forces on the nacelle of the

engine. Permanent changes in eccentricity, on the other hand, can be caused by uneven pressure distributions due to holes and slots cut into the casing for secondary systems such as bleed. Hard landings and stall events can also cause the blades to rub and thus remove material from one side of the casing and not the other. This again leads to permanent eccentricity.

The distribution of the tip-clearance around the annulus has a major effect on the efficiency and stall margin of a compressor. It is therefore important to understand the effect on the flow physics of having a larger gap on one side of the compressor than the other.

Graf et al. [2] presented a paper on this subject. They measured the stall margin of a single-stage compressor with stepwise cut-outs in the casing. Their results showed that this form of eccentric tip-clearance gives a stall margin penalty almost equivalent to having a concentric clearance equal in size to the maximum eccentric clearance. This finding is in line with the rule of thumb (Freeman [1]), that the stall margin of a compressor is determined by the maximum clearance.

In their paper, Graf et al. [2] adapted a two-dimensional model to capture the flow redistribution in a compressor with eccentric tip-clearance. They started by using a model for flow redistribution in a compressor with inlet distortion previously developed by Hynes and Greitzer [3]. This model uses the parallel compressor argument: The compressor is constrained to provide the same exit static pressure at all circumferential locations, so, given a uniform inlet total pressure, the total-to-static pressure rise must be constant around the annulus of the eccentric compressor. However, a compressor with a smaller tip-clearance will provide a higher pressure rise, at a given flow coefficient, than one with a larger tip-clearance. This means that the flow entering the compressor must redistribute itself upstream to give a higher flow coefficient in the small tip-clearance region and a lower flow coefficient in the large tip-clearance region. This is illustrated schematically in Fig. 1.

In this paper, it will be shown that the basic principles of the parallel compressor model do apply in the case of eccentric tip-clearance. However, the radial variation in flow rate is also important, and therefore a three-dimensional model must be used.

Tip-clearance eccentricity, and the associated flow redistribution, also influences the stall inception behaviour of a compressor. Researchers at Notre Dame University (Cameron et al. [4] and Bennington et al. [5]) studied the development of spike-type disturbances in a compressor with eccentric tip-clearance. Cameron et al. [4] showed that, very close to the stall point, spike-like disturbances appear in the region with the largest tip-clearance. These spikes then decay in the part of the annulus where the tip-clearance is smaller. Eventually, one of these growing and decaying disturbances completes an entire revolution of the annulus without fully decaying and then grows rapidly into a stall cell.

Bennington et al postulated that this phenomenon is due to the stronger tip-leakage vortex in the large tip-clearance sector (an idea proposed by Storer and Cumpsty [6]) causing stall inception to occur first at this location. They went on to develop a simple model which uses a momentum balance to try to predict the operating point at which stall will occur based on a model of the location of the tip-leakage vortex [5]. Their model contains many simplifications and relies heavily on empirical constants.

It is clear from the above discussion that tip-clearance eccentricity is of interest both in academia, where it may be useful in understanding the fundamentals of stall inception, and in industry, where it presents an exacting design challenge. It is therefore surprising that so little work has been done in this area.

A systematic study of the effects of clearance and eccentricity has been carried out on a single-stage compressor. From the trends in compressor behaviour over a wide range of clearance sizes, an improved understanding on which future design rules can be based is presented in this paper. In particular, an improvement to the rule of thumb will be presented.

The analytical model proposed by Graf et al. [2] will be compared with the experimental data and found wanting. Instead, improved understanding of the three-dimensional flowfield in an eccentric compressor will be provided by a model based on the Immersed Boundary Method with Smeared Geometry (IBMSG), as proposed by Cao et al. [7].

It will be shown that the radial component of the flow redistribution cannot be ignored, and that the IBMSG can be used to explain the three-dimensional nature of the flow redistribution in an eccentric compressor.

EXPERIMENTS

The experiments described in this paper were carried out on a single-stage, low-speed, high hub-tip ratio compressor in the Whittle Laboratory. A diagram of the compressor and its key operating parameters are given in Fig. 2. The blades are of controlled diffusion design with modifications to create a low-speed representation of a typical aero-engine high-pressure compressor stage (circa. 2000).

The compressor casing can be moved relative to the centreline of the rotor to give a sinusoidal variation in rotor tip-clearance around the annulus. (The effects discussed above tend to cause eccentricity which is stationary in the absolute frame – as opposed to rotating with the blades – and has a wavelength of one circumference, hence the choice of stationary, once-per-rev eccentricity for this study.) Moving the casing in this way maintains the same average clearance as the concentric case, and is more representative of realistic engine conditions than the stepped eccentricity investigated by Graf et al. [2]. The eccentricity was measured in each case using a dial gauge on the rotor to measure the change in clearance at 18 points round the annulus (accuracy: 5 microns). This arrangement is shown schematically in Fig. 3.

In this paper, eccentricity is quoted as a percentage of the average gap size:

$$\text{Eccentricity} = \frac{\epsilon_{max} - \epsilon_{min}}{\bar{\epsilon}} \times 100\% \qquad \textbf{(1)}$$

where ϵ denotes tip-clearance. Using this definition, a casing rub would correspond to an eccentricity of 200%, although levels of non-contact eccentricity of 50 – 75% are more common. These more common eccentricity levels will therefore be used in this work.

The average tip-clearance was also varied. This was done by cutting back the rotor blades. A rotary table and a milling machine were used for this purpose, providing a tip diameter uncertainty of less than 10 microns. In this paper, the average tip-clearance is varied systematically from 1.4% to 10% chord (the practical range of interest is up to 5%).

As the compressor is low-speed and the rotor has been balanced, the effects of rotor imbalance and shaft whirl are negligible. All values quoted are for the 'cold' case, i.e. measured prior to running the compressor. The effect of blade growth due to temperature and centripetal forces is roughly the same in all cases and has been estimated to be 0.07 mm on radius.

The stall point of each configuration was found by continually measuring the compressor performance as the throttle was closed (logging at 100 kHz and averaging every 100 ms). The flow coefficient and pressure rise were measured using six casing static pressure tappings far upstream of the rotor and far downstream of the stator, and using three inlet total pressure probes, as shown in Fig. 2. The stall point was taken to be the last measured point before the exit pressure drops (see red circle on Fig. 4 for an example). The mean stall point was taken from 5 runs for each configuration. For average clearances below 5% chord, the mean standard deviation of stall points was 0.3%, while it was 0.5% for larger gap sizes.

The stall inception behaviour of the compressor (spike or modal) was found using fast-response pressure transducers mounted near the rotor leading edge. The stalling behaviour of the compressor with the datum clearance is discussed in Pullan et al. [8], and is spike-type with the disturbance originating at the rotor tip. The question of whether the compressor exhibited part-or full-span rotating stall was answered by considering the in-stall part of the characteristic, as shown in Fig. 4: a large pressure drop from the un-stalled part of the characteristic to the in-stall level indicates full-span stall, while a smaller pressure drop and a smaller hysteresis loop indicates part-span stall, as shown by Day et al. [9]. A compressor in part-span stall will eventually drop into full-span stall if throttled further, as shown for the characteristic with 8.5% clearance (pink line on Fig. 4).

The circumferential flow coefficient variation at the rotor tips was found by measuring the local casing static pressure 0.5 rotor chords upstream of the rotor blade at eighteen positions around the annulus (the same 18 locations as used for the eccentricity measurements). The linearised Bernoulli equation was then used to deduce the variation in axial velocity. This was done at the design flow coefficient and near stall.

NUMERICAL MODELLING

When a compressor is operating with tip-clearance eccentricity, there is an inevitable flow redistribution around the annulus, i.e. the flow coefficient is not the same at all circumferential positions. In order to gain further insight into this redistribution, two numerical models will be used to simulate the flow in an eccentric compressor:

1. The two-dimensional (axial and circumferential) model of Graf et al. [2], adapted for a compressor without Inlet Guide Vanes (IGVs).
2. A three-dimensional (axial, circumferential and radial) Immersed Boundary Model with Smeared Geometry (IBMSG) solver, developed by Cao et al. [7], which uses an Euler code and loss correlations to model the compressor. The solver was adapted for this work to predict the behaviour of an eccentric compressor when given its concentric performance.

In this section, the models will be described; their accuracy relative to experimental data will be discussed in a later section.

Graf et al. [2] adapted the model of Hynes and Greitzer [3], which was developed for flow redistribution in a compressor operating with inlet distortion. This two-dimensional model starts by assuming that there is a variation in flow coefficient around the annulus. This means that the fluid in the rotor passages must be accelerating and decelerating as it moves through the changing flowfield, and this acceleration must be balanced by a corresponding pressure fluctuation. Graf thus gives the following equation:

$$\frac{p_2 - p_{01}}{\frac{1}{2}\rho U_{mid}^2} = \psi_{T-S}(\phi, \epsilon) - \lambda \frac{\partial \phi}{\partial \theta} \qquad \textbf{(2)}$$

where λ is an inertia parameter related to the rotor blade geometry.

This equation assumes that the rotor inlet angle is invariant. As the compressor used for the current study was tested without IGVs, this assumption is not valid. Thus the model needs to be extended to include the dependence of ψ_{T-S} on the absolute inlet flow angle, α. This situation has been considered by Longley [10], and a full derivation of the resulting expression for the flowfield in an eccentric machine can be found in Appendix A. For the sinusoidal tip-clearance variation considered in the current work, the final equation for the perturbation in flow coefficient around the annulus is:

$$\delta\phi = -\Delta\epsilon \frac{\partial \psi}{\partial \epsilon} \left[\frac{\frac{\partial \psi}{\partial \phi} \cos\theta - \left(\lambda - \frac{1}{\phi}\frac{\partial \psi}{\partial \alpha} \sin\theta\right)}{\left(\lambda - \frac{1}{\phi}\frac{\partial \psi}{\partial \alpha}\right)^2 + \left(\frac{\partial \psi}{\partial \phi}\right)^2} \right] \qquad \textbf{(3)}$$

It can be seen that the sinusoidal tip-clearance distribution leads to a variation in local flow coefficient (axial velocity) which is also sinusoidal, but that there is a phase lag, which is given by:

$$\Delta\theta = -\operatorname{atan}\left(\frac{\lambda - \frac{1}{\phi}\frac{\partial \psi}{\partial \alpha}}{\frac{\partial \psi}{\partial \phi}} \right) \qquad \textbf{(4)}$$

From the characteristics for the compressor with different levels of (concentric) tip-clearance, values for $\frac{\partial \psi}{\partial \epsilon}$ and $\frac{\partial \psi}{\partial \phi}$ were calculated. An expression for $\frac{\partial \psi}{\partial \alpha}$ was also found from extra experiments where IGVs were fitted temporarily and used to set the inlet flow angle at a series of values.

In order to provide more in-depth modelling, this time using a three-dimensional approach, the flow redistribution around the compressor was calculated using an Immersed Boundary Model with Smeared Geometry (IBMSG). This model was developed by Cao et al, and details of the model and its execution are discussed in Ref. [7]. The model smears the real blade geometry (represented by a camber line) into an infinite number of small blades (in practise this is discretised into the number of mesh cells within the blade zone). These smeared blades cause the flow to follow the real camber line in the blade frame of reference (rotor or stator as appropriate). In each mesh cell, the smeared blade is modelled using an immersed wall boundary (IBM); the direct forcing scheme is then applied to fulfil the slip wall condition. The body force imparted by the blade to the flow is thus modelled. In practise, the Euler equations are solved in a duct and the modelled body force is added as a source term into the momentum and energy equations within the blade zone.

The IBMSG solver was adapted for the present work so as to predict the performance of an eccentric compressor using only performance data from the concentric compressor. The drag coefficient (used for modelling the viscous body force) is expressed as a parabolic increase from the mid-span value at both hub and tip. The depth and extent of this high drag region are controlled independently at the hub and tip (as shown in Fig. 5), and all four coefficients were correlated to the size of the tip gap. This correlation was tuned to provide the same level of blockage as that observed in experimental measurements downstream of the rotor with concentric clearance.

An example of the tuning process is shown in Fig. 6, where rotor exit flow (measured from a hotwire traverse and pitchwise-averaged) is compared with the simulation outputs for three concentric cases. It can be seen that the level of loss is consistent between the simulations and experiments, though there is detail in the experimental data that the model does not capture, especially in the endwalls. (The aim is to generate the same level of concentric blockage in the hub and tip region, as a compressor design code would do.)

Given an eccentric clearance, the IBMSG solver used the concentric loss correlations described above to predict the behaviour of the flow around the annulus in both the spanwise and radial directions.

EFFECT OF ECCENTRICITY ON PERFORMANCE

Figure 7 shows the measured effect of eccentricity on the operating characteristic of the compressor for two levels of average clearance – Fig. 7(a) shows a comparison of concentric and eccentric builds with an average gap size of 1.7% chord, while Fig. 7(b) shows the characteristics for the compressor with an average clearance of 3.3% chord and different levels of eccentricity. It can be seen that, for a given average clearance size, tip-clearance eccentricity leads to an increase in stalling flow coefficient. It is also apparent that the compressor produces the same un-stalled total-to-static pressure rise regardless of eccentricity (i.e. all the characteristics lie on top of each other), but that stall occurs earlier as the level of eccentricity is increased. Even with a large average clearance (Fig. 7(b)), eccentricity does not lead to a loss of pressure rise. This shows that clearance eccentricity is fundamentally different from an increase in average clearance, which tends to cause a drop in pressure rise as well as an increase in stalling flow coefficient. (See the difference between the black lines in Figs 7(a) and 7(b) or compare the black and red lines in Fig. 4 – the concentric cases for 1.7% and 3.3% clearance: there is a clear drop in pressure rise with increasing gap).

The stalling flow coefficients of all the test cases (concentric as well as eccentric) are plotted against maximum tip-clearance in Fig. 8. It can be seen that there is a rapid increase in stalling flow coefficient with maximum tip-clearance for gap sizes from 1.1% to 3.5% chord. After this the stall point becomes roughly constant. This constant relationship between tip-clearance and stall point breaks down at a maximum tip-clearance of around 6% chord, which is when the compressor begins to exhibit part-span stall instead of going straight into full-span rotating stall (see Fig. 4 for examples of characteristics with full- and part-span stall at different clearances).

For all mean clearance levels, Fig. 8 demonstrates an increase in stalling flow coefficient with an increase in eccentricity. Figure 9 shows that this increase in stalling flow coefficient is approximately linear for small to moderate tip-clearances – the data points fit on straight lines. Also observable in Fig. 9 is the reduction in sensitivity to eccentricity with increased average clearance, i.e. the gradient of the straight line gets shallower as the average clearance increases. In fact, the gradient decreases linearly with average clearance size. (Again, this relationship breaks down at around 6% chord.)

Effect of eccentricity on stall inception mechanism

It is interesting to note that the stall inception mechanism of the test compressor is spike-type in the datum configuration, but changes to modal as the average clearance is increased (see Young [8] for a full discussion of the stall inception in both concentric and eccentric configurations). Spike-type stall was also observed in the eccentric tests with 1.7% average clearance. However, with mid-sized average clearances (2.4 - 4%) and eccentricity, the stall inception mechanism was less clear-cut, with long-lengthscale modal waves occurring in the large clearance sector of the compressor. These modal waves appeared to decay as they moved through the small tip-clearance sector of the compressor. As well as the modal disturbances in the large clearance sector of the annulus, spikes appeared just after the minimum clearance point and then decayed as they propagated. The final route into stall appears to be a combination of spike and modal stall inception. This is similar to the observations of Longley in compressors with inlet distortion [10].

With large tip-clearances, the stall inception mechanism became harder to identify, due to the formation of large disturbances in the large tip-clearance part of the annulus, which obscured the developing stall cell.

ACCOUNTING FOR ECCENTRICITY IN DESIGN RULES

It is often assumed that the stall point of an eccentric compressor will be the same as that of a concentric compressor with clearance equal to the maximum gap [1]. The logic behind this is that the large clearance part of the annulus will become unstable at the point at which an equivalent concentric compressor would stall, and that this instability will cause the eccentric machine to stall.

This ‘rule of thumb’ is used by designers to ensure that their compressor will be able to cope with the level of eccentricity they anticipate during operation. The rule of thumb can be tested using Fig. 8, where it can be seen that tests with the same maximum clearance do not necessarily have the same stall point. For example, a compressor with 1.7% mean clearance and 2.4% maximum clearance (top red circle) has

a lower stall flow coefficient than a concentric compressor with 2.4% mean clearance (blue and grey square just above red circle). This means that the maximum clearance is not a reliable indicator of the stall point of an eccentric compressor.

This is shown in more detail in Table 1, which compares the stall point of an eccentric compressor to that with concentric clearance but the same maximum gap size. For a compressor with 1.7% average clearance, the stall point penalty for eccentricity is only 60% of that incurred by increasing the clearance concentrically. The same calculation with a 2.4% mean clearance gives a discrepancy of 25% between eccentric and concentric compressors with the same maximum gap. This shows that the effect of eccentricity on the performance and stability of a compressor is not as simple as suggested by Freeman's rule of thumb [1].

Figure 10 shows the same set of data as Fig. 8, but the stalling flow coefficient is now plotted against the average clearance over a sector of 180° centred on the maximum tip-clearance. It can be seen that using this alternative definition of the maximum clearance causes all the test cases to collapse onto the spline fit for the concentric data (grey dashed line).

FLOWFIED REDISTRIBUTION

When a compressor is operating with tip-clearance eccentricity, there is an inevitable flow redistribution around the annulus, i.e. the local flow coefficient is not the same at all circumferential positions. In this section, the measured flow redistribution at the rotor inlet will be compared with two low-order models: the two-dimensional model of Graf et al. [2], adapted for a compressor without IGVs, and the three-dimensional Immersed Boundary Model with Smeared Geometry (IBMSG) solver of Cao et al. [7], adapted for an eccentric machine. Both models have been described in detail above.

The tip-clearance eccentricity studied here is seen by the rotor as a once-per-revolution disturbance to which the compressor responds quasi-steadily. This means that the response should only contain the first harmonic. Therefore, to aid comparison, the experimental results have been plotted using the first Fourier harmonic (amplitude and phase) of the raw data; the red circles on Figs 11 and 12 simply denote the measurement locations. An example of the raw experimental data with error bars is given in Appendix B.

As described in the methods section above, the experimental data is taken from casing static pressure tappings 0.5 rotor chords upstream of the rotor inlet plane. (The rotor tip flow variation is of most interest in terms of compressor stability as this is where stall is known to begin in the compressor used here, at least for the smaller clearance cases.)

Two-dimensional model

A comparison of the two-dimensional model of Graf with the experimental data for a compressor with 1.7% average clearance and 75% eccentricity is shown in Fig. 11 (a), which is a plot of flow coefficient against circumferential position. The first harmonic of the experimental data is shown in red, while the output of the Graf model is shown in black, and the circumferential location of the maximum gap is denoted by the green dotted line. Data is shown for two operating points: design ($\bar{\phi}$= 0.50), and near stall ($\bar{\phi}$ = 0.43).

As shown in Equation 3, the sinusoidal tip-clearance variation is expected to give rise to a sinusoidal flow coefficient variation around the annulus. Comparing the blue and red lines on Fig. 11 (a), it can be seen that the Graf model predicts virtually no flow redistribution at the design point (top lines in Fig. 11 (a)), while the experimental data shows a significant redistribution. At near stall conditions – lower lines – the Graf model predicts the amplitude of the flow redistribution (i.e. the peak to trough height of the sine wave) to be roughly half the experimental value at near stall conditions. It is also important to note that the phase lag is not predicted correctly by the Graf model at either operating point.

For larger clearance cases (results not shown), the amplitude of the flow redistribution was also under-predicted by the Graf model, while the phase lag was over-predicted. At this point, it is worth noting that the results presented by Graf et al. in their paper [2] also reveal a disagreement in phase lag between measurement and theory.

It should also be pointed out that the model of Graf et al. assumes that the flow can be considered as uniform across the span, i.e. a two-dimensional approach. In reality, however, the disturbance which causes the flow redistribution (tip-clearance eccentricity) is not uniform across the span, but is applied only at the outer radius. (The original model was for inlet distortion [3], which is often applied evenly across the span.)

Three-dimensional model

Turning now to the results of the IBMSG model, Fig. 11 (b) shows that the data from the tip region (black lines – again taken 0.5 chords upstream of the rotor) agrees more closely with the experimental measurements than the Graf model (blue line), and the IBMSG gives good agreement both in terms of the amplitude and phase lag of the flow redistribution at the tip. To illustrate this further, the flowfield redistribution with a larger clearance is shown in Fig. 12. Good agreement is again observed.

A summary of all the cases used for validation of the IBMSG model is shown in Fig. 13, which is a plot of the amplitude of the flow redistribution (i.e. peak to trough height of the sine wave) for each test case. The cases include a variety of levels of average clearance and eccentricity. It can be seen that the agreement in the amplitude of the flow redistribution between the experimental data and the IBMSG simulations is reasonable, though there is significant scatter in the experimental data. It can also be seen in Fig. 13 that the model predicts a linear increase in redistribution amplitude (i.e. the range of flow coefficients at the tip) with increasing clearance variation – regardless of average clearance size.

The IBMSG is a three-dimensional model, and thus is able to predict flow redistribution in both the circumferential and radial directions. Figure 14 shows the rotor exit flow coefficient measured in the maximum and minimum tip-clearance of the compressor in an eccentric configuration. As in Fig. 6, data from the IBMSG is compared to pitchwise-averaged results from a hotwire traverse in the compressor. It can be seen that the model captures the trends well, with higher flow rate in the hub region of the compressor. (As detailed in the modelling section above, the aim is not to capture the details of the endwall regions, but to achieve the correct overall loss magnitude at the hub and tip). This data gives confidence that the IBMSG model is capturing the flow redistribution across the span as well as in the tip region.

Turning now to the flow at the compressor inlet, Fig. 15 shows the rotor inlet flow variation as simulated by the IBMSG for a compressor with 3.3% clearance and 75% eccentricity. This is a contour plot of rotor inlet flow coefficient around the entire annulus, with the maximum clearance on the right and the minimum clearance on the left. It can be seen that the flow rate is highest at point A, which is on the hub just after the minimum tip-clearance, and lowest at point B, which is at the tip just after the maximum tip-clearance.

It can also be seen in Fig. 15 that there is a large variation in flow coefficient across the span, and that the phase lag of the redistribution also varies with span (compare the locations of the maximum flow coefficient at hub and tip – points A and C). The change in flow coefficient between the hub and the tip is almost as large as the variation around the annulus, and the phase lag varies by almost 15°. All this shows that the spanwise-uniform assumption of Graf et al. is invalid, and that spanwise effects cannot be neglected. (Note: the code uses concentric design data as input, and is computationally cheap enough to be used for design calculations.)

The changes in flow coefficient around the annulus mean that the relative flow angle is varying at rotor inlet. In a compressor with no IGVs, the absolute flow angle at rotor inlet will also change (as fluid moves circumferentially upstream of the rotors). This combined effect can be seen in Fig. 16, which gives contours of rotor incidence in a compressor with 3.3% average clearance and 75% eccentricity operating at near stall conditions. It can be seen that the tip incidence is 1.5 degrees higher in the maximum clearance sector of the compressor than the minimum clearance region, meaning that the blades are significantly closer to stall in one part of the annulus than the other.

EFFECT OF ECCENTRICITY ON STABILITY

The flow redistribution discussed in the previous section means that the operating point of the compressor is varying around the annulus, so that some parts of the annulus are closer to stall than others. Further to this, when viewed as an axisymmetric compressor, the sector with the large clearance would naturally stall at a higher flow coefficient than the sector with the small clearance. This leads to the definition of an 'equivalent concentric stall point', i.e. the point at which a particular part of the annulus would stall if it were to be operating as a concentric compressor with the same clearance.

The relationship between the concentric stall point and the size of the tip-clearance was found from the performance characteristics of the compressor with concentric clearances ranging from 1% to 5% chord. As shown on Fig. 8, the stalling flow coefficient increases sharply from 1.5 to 3.3% chord and then becomes constant for clearances larger than this – all these concentric cases are highlighted in grey in Fig. 8. A

dotted curve has been fitted through these points. From this curve, the equivalent concentric stalling flow coefficient was estimated for every circumferential position around the annulus for various levels of average clearance and eccentricity.

In conjunction with the local flow coefficient, the local equivalent concentric stall point can be used to investigate the stability around the annulus of the compressor. At a given circumferential location, if the local flow coefficient is lower than the equivalent concentric stall point, that part of the annulus can be considered to be locally unstable.

The local flow coefficient at the tip (taken from IBMSG simulations) just before stall, with 1.7% average clearance, has been plotted as a solid line for different levels of eccentricity in Fig. 17 (a). (As stated above, the tip flowfield has been chosen because the compressor is known to stall from the rotor tip.) In addition, the local equivalent concentric stall point is plotted as a dashed line for each case.

Comparing the local flow coefficient with the equivalent concentric stall point, it can be seen that there is a part of the annulus in which the compressor is forced to operate at flow coefficients below the stability limit of a concentric compressor with the same local tip-clearance. It appears, therefore, that the large clearance part of the annulus is being stabilised by the small clearance sector. Considering the data with three different levels of eccentricity, shown in Fig. 17 (a), it can be seen that the circumferential extent of this unstable sector is approximately constant at stall.

Figures 17 (b) and (c) show the same family of graphs but for larger average tip-clearances. It can be seen that the extent of the unstable sector increases with clearance, from 114^o with 1.7% clearance to 146^o with 3.3% clearance. For a given level of clearance, however, the unsteady sector size is approximately the same for all levels of eccentricity.

Figure 18 is a bar chart of the unstable sector size at stall for all nine test cases shown in Fig. 17. In Fig. 18, it can be seen that the unstable sector size is relatively unaffected by eccentricity, but the mean value increases linearly with clearance size (red line).

A possible reason for the traditional rule of thumb being pessimistic might be explained from the data presented here: in an eccentric compressor, there is a circumferential variation in both local equivalent stall point and local flow coefficient, such that one part of the annulus is forced to operate beyond its local stalling flow coefficient. The less stable part of the annulus is therefore stabilised by the other part of the annulus, which is operating with considerable stability margin. When the unstable sector reaches a critical size, the stable (small clearance) sector can no longer stabilise the compressor and thus the machine goes into rotating stall.

Based on the unstable sector sizes shown in Fig. 18 (114^o, 128^o, 146^o), it is tempting to try to propose a new rule of thumb linking the size of the unstable sector to the stability of the compressor. However, with the limited amount of data available, it is simpler to improve the traditional rule of thumb by using the average clearance of the worst 180^o sector rather than the worst clearance itself. The improvement brought about by this simple approach has been shown above (compare Figs. 8 and 10).

CONCLUSIONS

The effects of eccentricity and tip-clearance have been investigated on a single-stage compressor using both experimental data and numerical modelling. The results show interesting trends and give insight into the flow that has not been reported before. In particular:

1. Tip-clearance eccentricity has been confirmed to affect the stall point of a compressor, but not the pressure rise. For a given level of average clearance, the stalling flow coefficient has been shown to increase linearly with eccentricity.
2. The established rule of thumb for eccentricity is that the stall margin of an eccentric compressor will be the same as that of a concentric compressor with a uniform clearance equal to the maximum eccentric clearance. Results in this paper show that this rule of thumb is overly pessimistic and the increase in stalling flow coefficient due to eccentric tip-clearance is as much as 40% smaller than that due to having a concentric clearance with the same maximum gap size.
3. Eccentricity leads to a redistribution of the flow at the compressor inlet. The two-dimensional (spanwise-uniform) model of Graf et al. [2] for flow redistribution has been compared with experimental results and discrepancies have been observed in both the magnitude and phase of the flow variation.
4. A new, three-dimensional model, based on the Immersed Boundary Model with Smeared Geometry (IBMSG), has been shown to represent the flow redistribution more accurately. This model uses concentric loss correlations, available at the design stage, to calculate the flow successfully in an eccentric machine.
5. Data from the IBMSG simulations also suggest a significant spanwise variation in terms of both the amplitude and phase lag of the flow redistribution (and likewise the incidence variation). This is the first time that the radial influence of tip-clearance eccentricity has been highlighted.
6. Experiments and the IBMSG model demonstrate that the amplitude of the flow redistribution in an eccentric compressor increases linearly with tip-clearance variation, regardless of average clearance size.
7. It has been shown that, near stall in an eccentric compressor, a substantial sector of the annulus will operate at a lower flow coefficient than the stability limit of a concentric compressor with the same local clearance. It can therefore be said that the small tip-clearance sector of the annulus has a stabilising effect on the large clearance sector and this restrains the compressor from going into stall.
8. For a fixed average clearance, the size of the sector operating beyond its equivalent concentric stalling point is observed to be constant at the stability limit, regardless of the level of eccentricity. Furthermore, a compressor with a larger average gap can tolerate a larger unstable sector before stalling.
9. For the compressor tested here, it has been shown that the traditional rule of thumb for estimating the effect of eccentricity on stall margin can be improved by using the average clearance in the worst 180^{o} sector rather than the actual clearance at the worst point.

NOMENCLATURE

Greek Letters

α	Absolute flow angle
ϵ	Tip-clearance gap
θ	Circumferential Coordinate/direction
λ	Inertia Parameter
ρ	Density
$\phi(\theta,r)$	Flow coefficient = $V_x(\theta,r)/U_{mid}$
ψ_{T-S}	Total-to-static pressure rise coefficient = $\frac{P_2 - P_{01}}{1/2 \rho U_{mid}^2}$

Roman Letters

A_n, B_n	Fourier coefficients
n	Harmonic number
P	Pressure
r	Radius, radial co-ordinate
U	Blade speed
V	Velocity

Subscripts

max/min	Maximum/minimum
mid	Mid-span value
x	Axial coordinate/direction
0	Stagnation quantity
¯	Mean quantity

ACKNOWLEDGMENTS

The authors thank Rolls-Royce, the EPSRC and the Maudslay Society for the funding that made this research possible. Thanks are also due to Dr John Adamczyk, Prof. Nick Cumpsty and Dr Chris Freeman for their help and input.

REFERENCES

1. Freeman, C. “Tip clearance effects in axial turbomachines.” VKI Lecture Series, April 1985.
2. Graf, M. B, Wong, T. S., Greitzer, E. M., Marble, F. E., Tan, C. S., Shin, H.-W. and Wisler, D. C., 1998. “Effects of Non-axisymmetric Tip Clearance on Axial Compressor Performance and Stability”. *ASME J. Turbomach.*, ***120***, Oct, pp 648 – 661.

3. Hynes, T. P. and Greitzer, E. M., 1987. "A Method for Assessing Effects of Circumferential Flow Distortion on Compressor Stability". *ASME J. Turbomach.*, ***109***, Jul pp 371 – 379.
4. Bennington, M. A., Ross, M. H., Cameron, J. D., Morris, S. C., Du, J., Lin, F, and Chen, J., 2010. "An Experimental and Computational Investigation of Tip Clearance Flow and its Impact on Stall Inception." In Proceedings of ASME Turbo Expo 2010, Jun 14-18, Glasgow, UK, GT2010-23516.
5. Cameron, J. D., Bennington, M. A., Ross, M. H., Morris, S.C. and Corke, T.C., 2007. "Effects of steady tip-clearance eccentricity and rotor whirl on stall inception in an axial compressor. In Proc. ASME Turbo Expo, May 14-17, Montreal, Canada, GT2007-28278.
6. Storer, J. A. and Cumpsty, N. A., 1994. "An approximate analysis and prediction method for tip clearance loss in axial compressors". *ASME J. Turbomach.*, ***116***, Oct pp 648 – 656.
7. Cao, T., Hield, P. and Tucker, P. G., 2016, Hierarchical Immersed Boundary Method with Smeared Geometry, AIAA SciTech forum and Exposition, 4 - 8 Jan 2016 in San Diego, California, USA.
8. Pullan, G., Young, A.M., Day, I.J., Greitzer, E.M. and Spakovszky, Z.S., 2015. "Origins and structure of spike-type rotating stall". *ASME J. Turbomach.*, 137(5), p.051007.
9. Day, I.J., Greitzer, E.M. and Cumpsty, N.A., 1978. "Prediction of compressor performance in rotating stall". *ASME J. Eng. for Gas Turbines and Power*, 100(1), pp.1-12.
10. Longley, J. P., 1990. "Measured and predicted effects of inlet distortion on axial compressors." In Proc. ASME Gas Turbine and Aeroengine Congress and Exposition, Jun 11-14, Brussels, Belgium. 90-GT-214.
11. Longley, J. P., 1994. "A Review of Nonsteady Flow Models for Compressor Stability". *ASME J. Turbomach.* **116**(2):202-215.
12. Young, A. M. "Tip-clearance Effects in Axial Compressors", 2012, PhD Thesis, University of Cambridge.

APPENDIX A – DERIVATION OF FLOW REDISTRIBUTION MODEL AFTER GRAF ET AL. [2]

The Hynes-Greitzer model [3], as adapted by Graf et al. for eccentric tip-clearance [2], starts by assuming that there is a variation in flow coefficient around the annulus. As the test compressor used in this work was not fitted with Inlet Guide Vanes, the stage pressure rise is stage pressure rise is not only a function of flow coefficient and tip-clearance but also of inlet angle, α. Thus equation **(2)** becomes:

$$\frac{p_2 - p_{01}}{\frac{1}{2}\rho U_{mid}^2} = \psi_{T-S}(\phi, \epsilon, \alpha) - \lambda \frac{\partial \phi}{\partial \theta} \qquad \textbf{(A1)}$$

Where λ is an inertia parameter related to compressor geometry:

$$\lambda = \frac{\text{Axial chord/radius}}{\frac{1}{2}\cos^2(\text{stagger})} \qquad \textbf{(A2)}$$

For small perturbations, this becomes:

$$\frac{\delta p_2 - \delta p_{01}}{\frac{1}{2}\rho U_{mid}^2} = \frac{\partial \psi}{\partial \phi}\delta\phi + \frac{\partial \psi}{\partial \epsilon}\delta\epsilon + \frac{\partial \psi}{\partial \alpha}\delta\alpha - \lambda \frac{\partial(\delta\phi)}{\partial \theta} \qquad \textbf{(A3)}$$

The inlet total pressure is fixed and thus cannot change around the annulus, and the same is true of the exit static pressure. This means that the left-hand side of the equation is zero, thus:

$$\lambda \frac{\partial(\delta\phi)}{\partial \theta} - \frac{\partial \psi}{\partial \phi}\delta\phi - \frac{\partial \psi}{\partial \alpha}\delta\alpha = \frac{\partial \psi}{\partial \epsilon}\delta\epsilon \qquad \textbf{(A4)}$$

The tip-clearance distribution can then be expressed as a Fourier series:

$$\delta\epsilon = \sum_{\substack{n=-\infty \\ n\neq 0}}^{n=\infty} A_n e^{in\theta} \quad \textbf{(A5)}$$

Where in this case $\delta\epsilon = \Delta\epsilon \cos\theta$, so $A_n = \frac{\Delta\epsilon}{2}$ for $n = \pm 1$ and all other terms are zero. The Hynes-Greitzer model is two-dimensional, and so any radial variations in the flowfield are ignored. Furthermore, the flowfield must be periodic in the tangential direction and perturbations from the mean flow coefficient must decay upstream of the rotor bladerow. This means that the velocity potential, Φ, of the flowfield is of the form:

$$\Phi = \sum_{n=-\infty}^{n=\infty} B_n e^{in\theta + |n|\frac{x}{r}} \quad \textbf{(A6)}$$

Where B_n are unknown Fourier coefficients (the $|n|\frac{x}{r}$ term explains why higher harmonics decay more quickly). By considering the relationship between the velocity field and the velocity potential in cylindrical polar co-ordinates and differentiating, it is found that:

$$\delta\phi = \sum_{\substack{n=-\infty \\ n\neq 0}}^{n=\infty} A_n e^{in\theta} \frac{\frac{\partial\psi}{\partial\epsilon}}{\left(\lambda n - \frac{1}{\phi}\frac{|n|}{n}\frac{\partial\psi}{\partial\alpha}\right)i - \frac{\partial\psi}{\partial\phi}} \quad \textbf{(A7)}$$

Substituting the Fourier coefficients for the tip-clearance distribution into this equation gives:

$$\delta\phi = -\Delta\epsilon \frac{\partial\psi}{\partial\epsilon}\left[\frac{\frac{\partial\psi}{\partial\phi}\cos\theta - \left(\lambda - \frac{1}{\phi}\frac{\partial\psi}{\partial\alpha}\sin\theta\right)}{\left(\lambda - \frac{1}{\phi}\frac{\partial\psi}{\partial\alpha}\right)^2 + \left(\frac{\partial\psi}{\partial\phi}\right)^2}\right] \quad \textbf{(A8)}$$

For full details of the linearisation process, see Longley [11], and for details of the treatment of inlet swirl sensitivity $\left({}^{\partial\psi}/_{\partial\alpha}\right)$, see Longley [10] and Young [12].

APPENDIX B – RAW EXPERIMENTAL RESULTS

All the experimental data for flow redistribution shown in the paper has been reconstructed from the first spatial harmonic of the raw measurements from 18 static pressure tappings around the annulus. In Fig. 19 the raw data is compared to the first spatial harmonic. It can be seen that there are no discernible higher order harmonics in the raw data, and the discrepancies between the reconstructed flow distribution and the raw data are all within the error bars.

Figure 10 thus	Eccentricity (%)	Max Gap (% chord)	Stall point	
1.7	0	1.7	0.406	
1.7	75	2.4	0.425	} Same max gap, different stall point
2.4	0	2.4	0.438	
2.4	75	3.3	0.452	}
3.3	0	3.3	0.457	

Table 1: Stalling flow coefficient of eccentric and concentric compressors with the same maximum clearance.

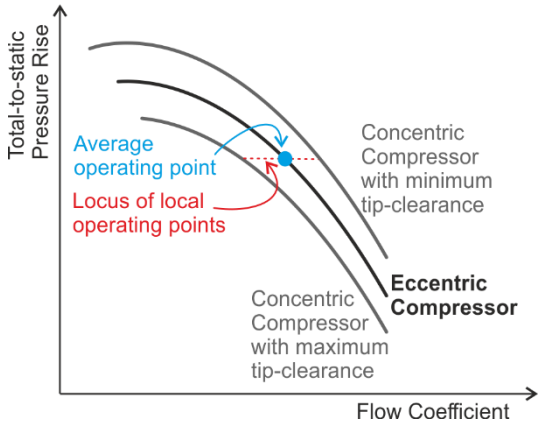

Figure 1: Flow coefficient variation around a compressor with eccentric clearance.

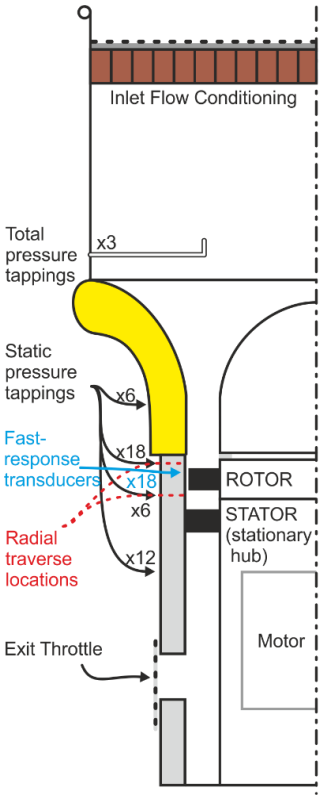

Rotor Tip diameter	488 mm
Hub-to-tip ratio	0.75
Blade count (rotor, stator)	58,56
Rotor stagger (hub, setting angle)	22°
Stator stagger (hub, setting angle)	35°
Rotor chord (true chord)	36 mm
Rotor tip-clearance (datum)	0.6 mm (1.7% chord)
Rotational speed	2980 rpm
Rotor Reynolds' number (chord)	1.7×10^5
Design flow coefficient	0.5
Design pressure rise coefficient	0.57

Figure 2: Key parameters of the test compressor.

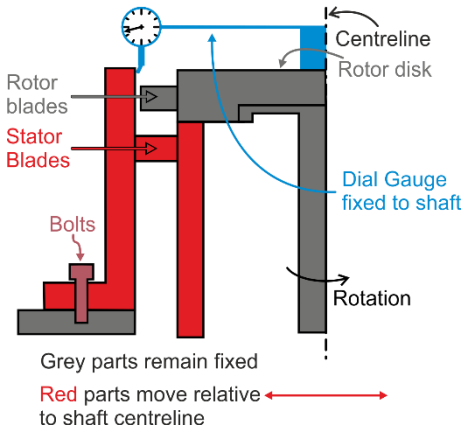

Figure 3: Schematic of eccentricity adjustment procedure: rotor remains fixed while casing moves; dial gauge is used to measure casing offset relative to shaft.

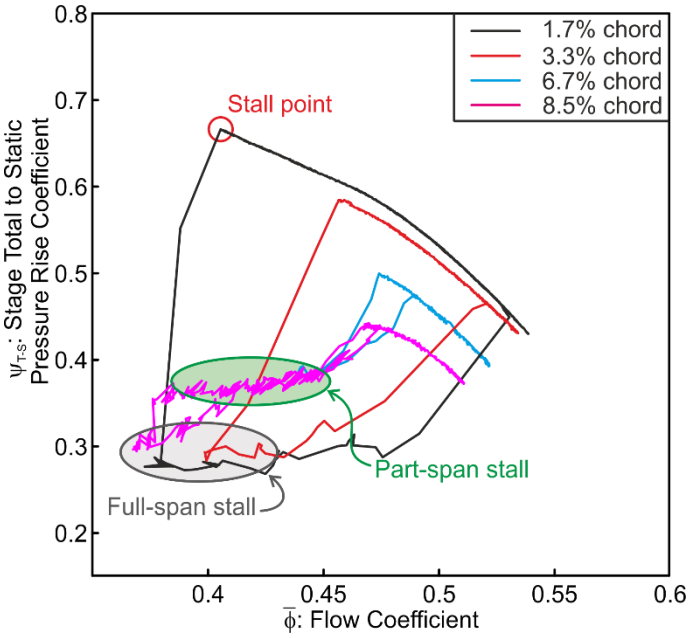

Figure 4: Characteristics with different levels of clearance (concentric), showing stall point and both full- and part-span hysteresis loops.

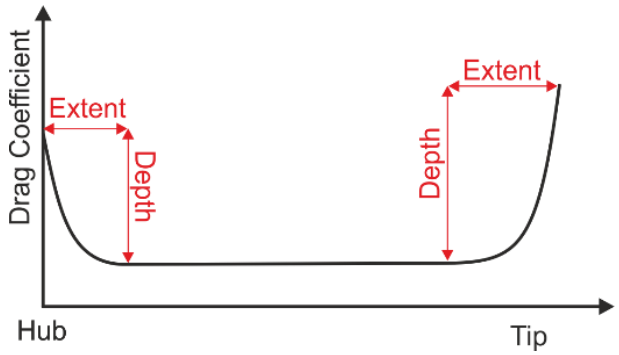

Figure 5: Sketch of control of high drag regions in hub and tip region used for IBMSG calibration.

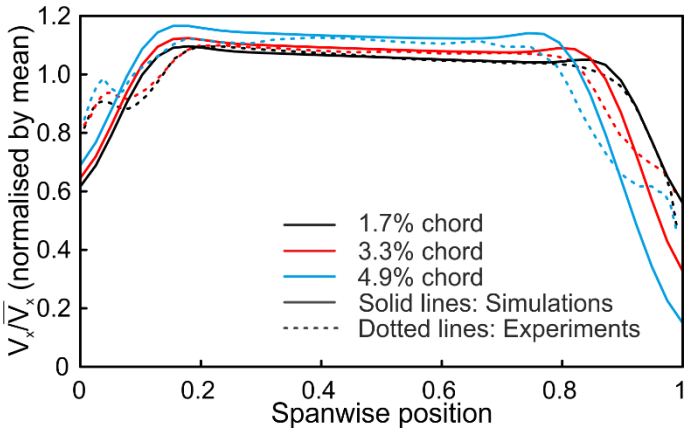

Figure 6: Effect of clearance on spanwise rotor exit flow variation (concentric cases used for calibration of IBMSG drag forces).

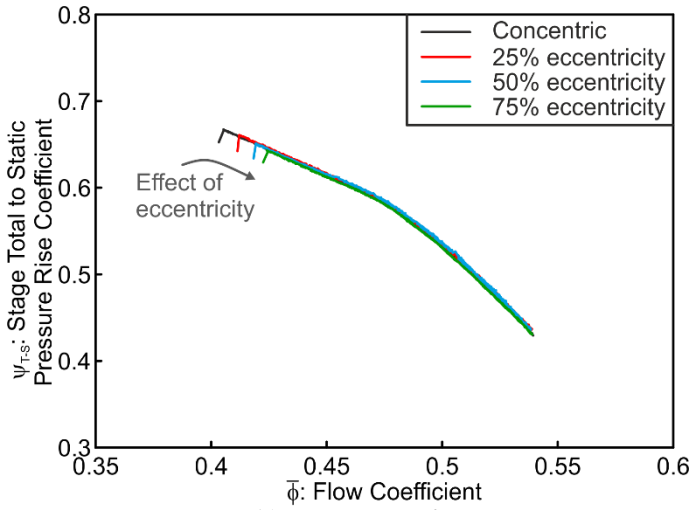

(a) 1.7% average clearance.

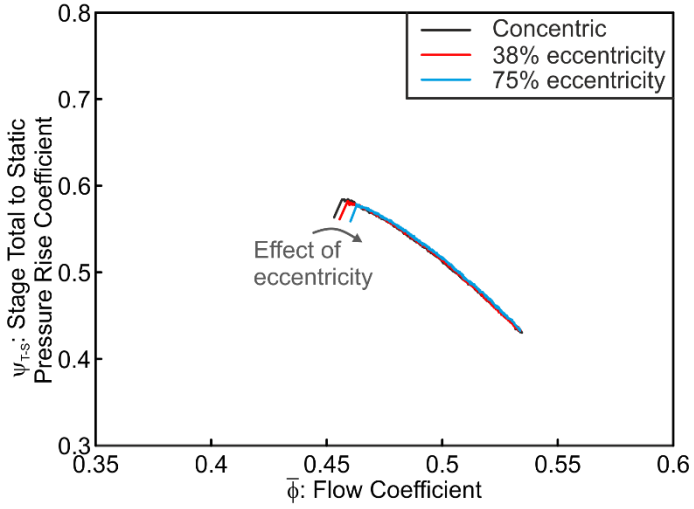

(b) 3.3% average clearance.

Figure 7: Effect of eccentricity on compressor characteristic with two levels of average clearance.

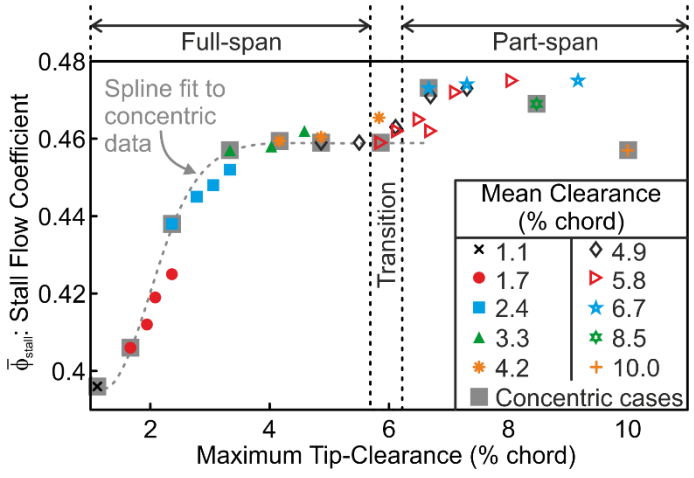

Figure 8: Stalling flow coefficient against maximum tip-clearance for all configurations tested.

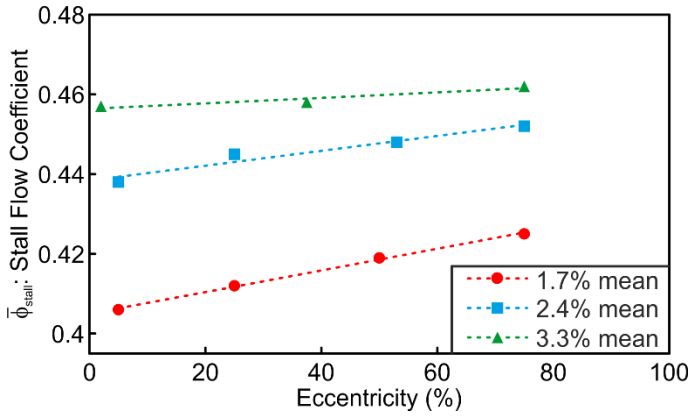

Figure 9: Stalling flow coefficient against eccentricity for three mean levels of clearance.

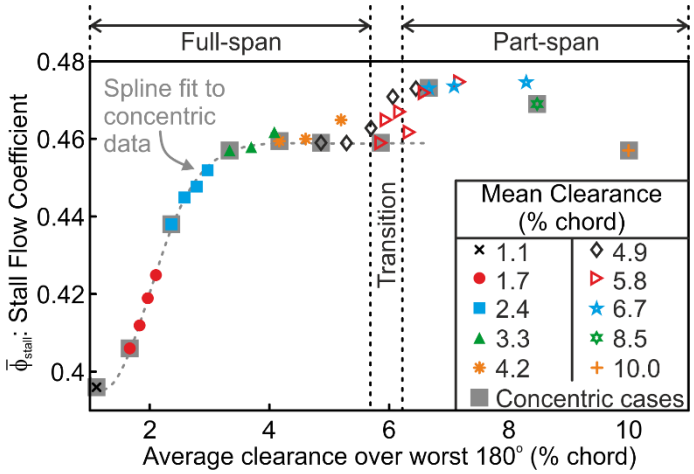

Figure 10: Stalling flow coefficient against clearance averaged over a sector of 180° centred on maximum clearance point.

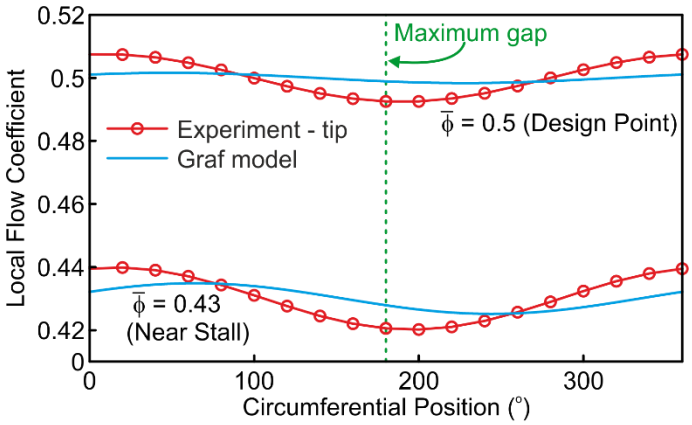

(a) Comparison of experiments with Graf model.

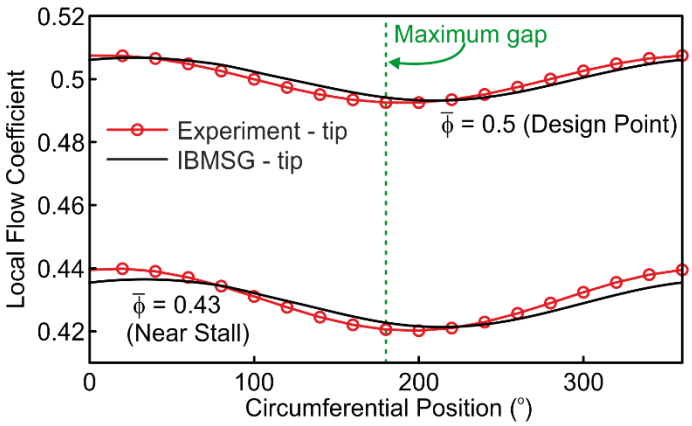

(b) Comparison of experiments with IBMSG results.

Figure 11: Measured and modelled flow coefficient variations with 1.7% clearance and 75% eccentricity (at two operating points).

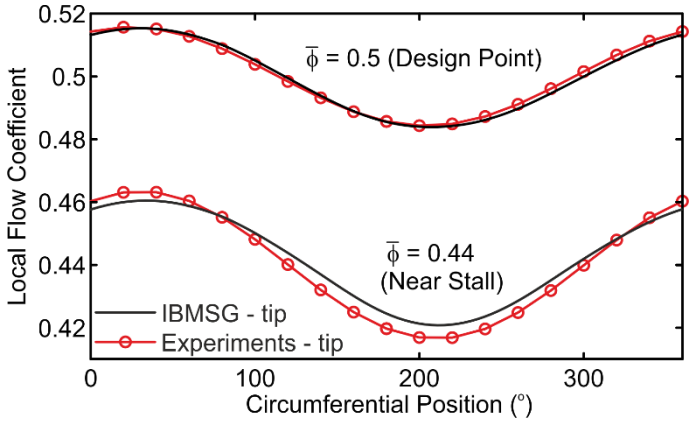

Figure 12: Measured and modelled tip flow coefficient variation in a compressor with 3.3% clearance and 75% eccentricity at two different flow coefficients.

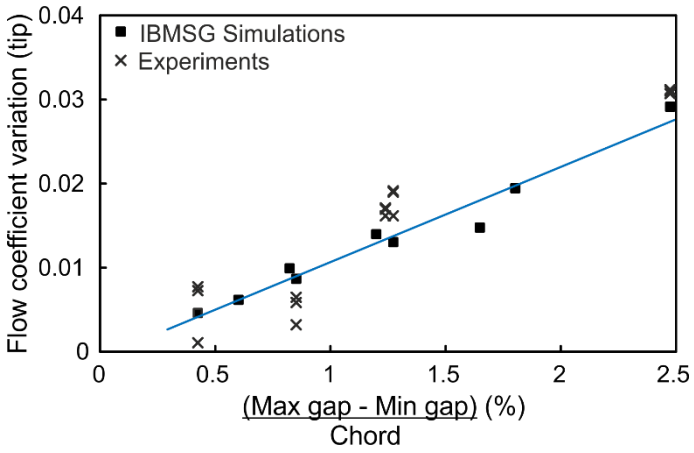

Figure 13: Comparison of amplitude of tip flowfield redistribution from experimental data and IBMSG model for a range of cases with different clearance sizes and eccentricity levels ($\bar{\phi}$ = 0.5).

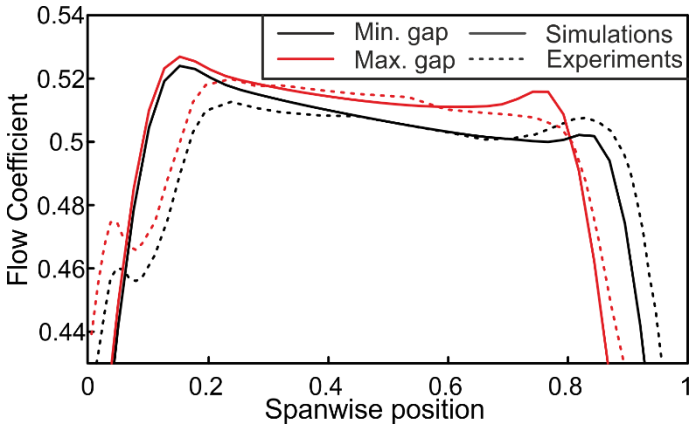

Figure 14: Comparison spanwise variation in rotor exit flow coefficient from experimental data and IBMSG model in the maximum and minimum gap of an eccentric compressor (3.3% clearance, 75% eccentricity, $\bar{\phi}$ = 0.5).

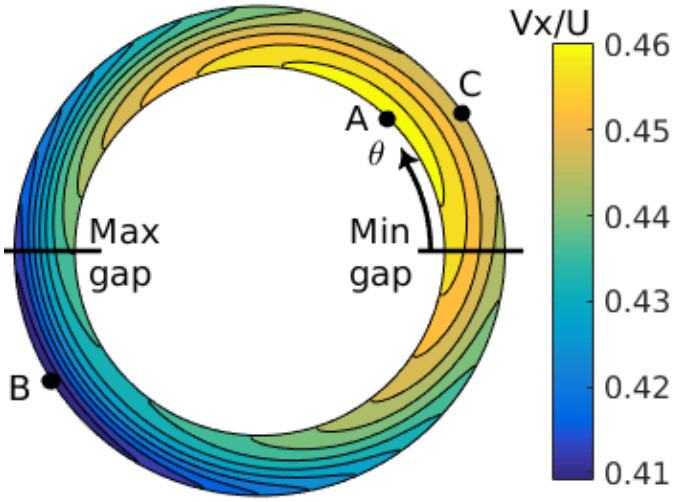

Figure 15: Contour plot of rotor inlet flow coefficient near stall taken from IBMSG simulation, 3.3% clearance 75% eccentricity.

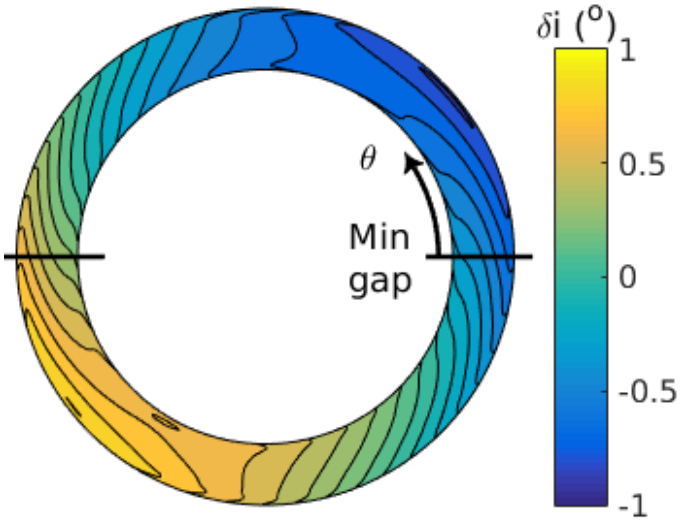

Figure 16: Contours of incidence change (incidence minus mean value at that radius) taken from IBMSG simulation, 3.3% clearance, 75% eccentricity.

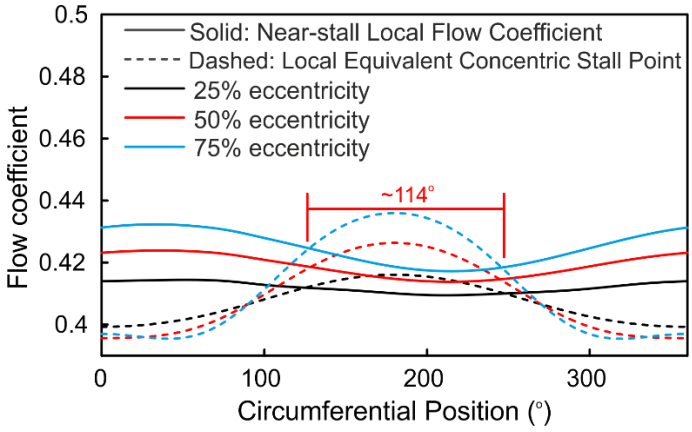

(a) 1.7 % average clearance.

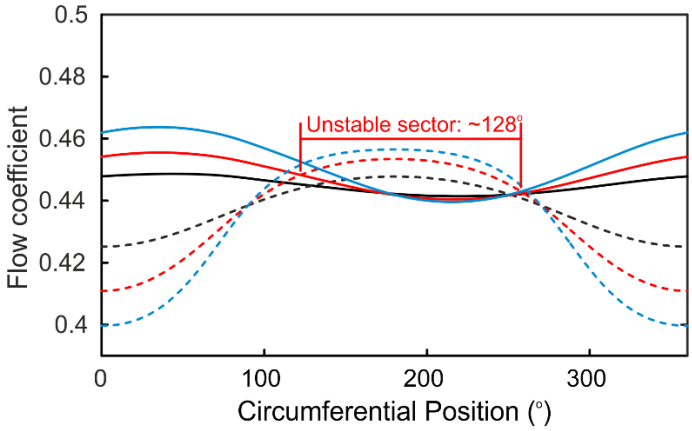

(b) 2.4 % average clearance.

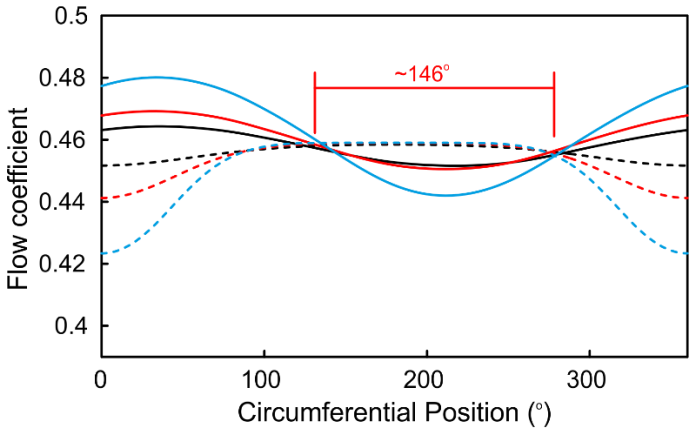

(c) 3.3 % average clearance.

Figure 17: Comparison of local inlet flow coefficient (IBMSG simulations at tip) and stall point for three levels of clearance.

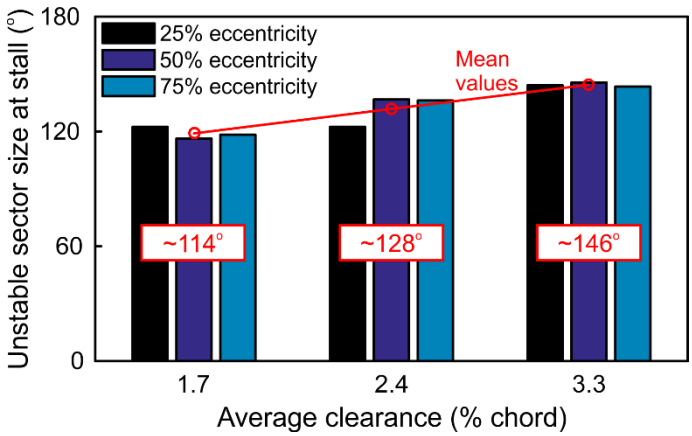

Figure 18: Unstable sector size at stall against average clearance.

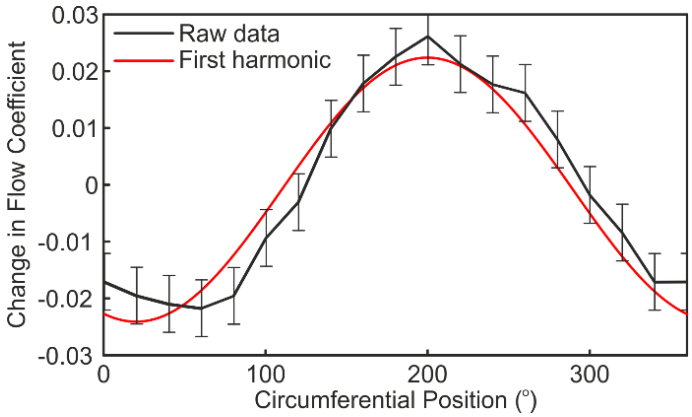

Figure 19: Comparison of raw flow coefficient measurements with the distribution reconstructed from the first spatial harmonic.

